Quantum-well and tight-binding analyses of spin-polarized photoemission from Ag/Fe(001) overlayers

N. V. Smith
AT&T Bell Laboratories, Murray Hill, New Jersey 07974

N. B. Brookes, Y. Chang, and P. D. Johnson
Physics Department, Brookhaven National Laboratory, Upton, New York 11973
(Received 26 July 1993; revised manuscript received 20 October 1993)

Spin-polarized photoemission experiments on expitaxial Ag overlayers on Fe(001) have shown that a minority-spin surface state of the bare substrate evolves into an interface state, moves to higher energies, and crosses the Fermi level E_F between 3 and 4 Ag monolayers. Application of a phase accumulation model shows that this state is a quantum-well (QW) state characterized by the quantum number $\nu=1$, where $\nu=m-n$, and where n and m are the number of wave-function nodes and number of layers, respectively. Higher members of the QW series cross E_F with a periodicity $\Delta m=(1-k_F/k_{BZ})^{-1}$ identical with that in recent theories for the alternation between ferromagnetic and antiferromagnetic coupling in magnetic multilayers. The QW model fails at low coverages. A tight-binding model captures the behavior at low coverages while reproducing QW behavior at high coverages.

I. INTRODUCTION

Multilayer structures composed of alternating ferromagnetic and nonmagnetic metals display intriguing properties.[1–3] The exchange interaction between successive magnetic layers can alternate between antiferromagnetic and ferromagnetic with increasing thickness of the nonmagnetic spacer layer. These effects are accompanied by giant magnetoresistance which makes such materials attractive to the magnetic recording industry. A principal question is the largeness of the period for alternation of the exchange coupling (10–20 Å) compared with the small period of, say, the oscillations of the Ruderman-Kittel-Kasuya-Yosida (RKKY) exchange function ($\sim$2 Å). In this paper, we examine results obtained in photoemission studies of these systems. In particular, data obtained from the Ag/Fe(001) system[4–8] are interpreted in terms of quantum-well (QW) and tight-binding (TB) models.

Fe/Ag is an attractive system for study for two reasons. First, there is a good lattice match between fcc Ag(001) and bcc Fe(001), and therefore good prospects for epitaxial growth of each metal on the other. Second, the Ag 4*d* bands lie as much as 4 eV below the Fermi level E_F, enabling a clear separation of them from the Fe 3*d* bands. The actual energy bands[9] along the Δ directions (appropriate to normal emission from the 001 faces) are shown in Fig. 1 for Ag and Fe for both majority and minority spin. Above the *d* bands, the relevant Δ_1 band for Ag is a propagating free-electron-like band. It is this feature that permits a simple quantum-well discussion. Other salient features are the Δ_1 *s-d* hybridization gaps in the Fe band structures. These are shown as the toned regions in Fig. 1. Propagating electron states are forbidden in these regions, and it is this fact that provides the possibility of confinement within a quantum well.

The format of this paper is as follows. In Sec. II, we assemble the pertinent experimental evidence. In Secs. III and IV we offer interpretation of the data from two viewpoints, a quantum-well analysis and a tight-binding simulation. Our QW analysis is similar to that presented earlier by Ortega *et al.*, but makes no use of the envelope function and carrier wave used in that model.[6] The QW model accounts nicely for the high Ag-coverage regime, but fails in the low-coverage and bare-substrate regimes. The TB model, on the other hand, is able to handle all regimes.

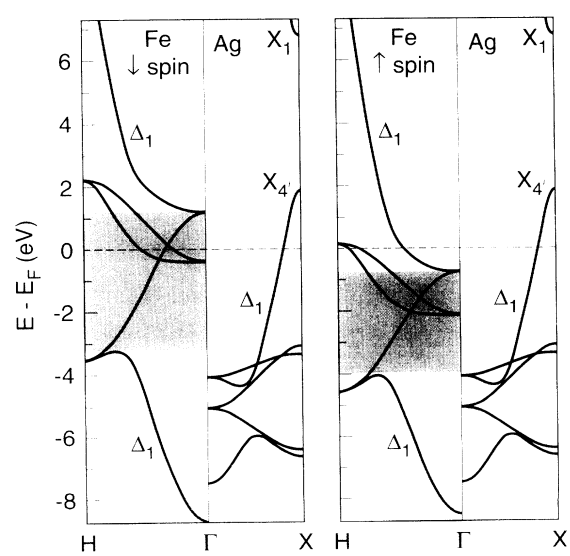

FIG. 1. Energy bands of Fe and Ag along the Δ direction for both minority (↓) and majority (↑) spins. The toned areas indicate the range of the *s-d* hybridization gap in Fe for states of Δ_1 symmetry.

 ©1994 The American Physical Society

II. EXPERIMENTAL SITUATION

We present in this section a brief discussion of the experimental results[4–8,10] relevant to our analysis.

A. Spin-polarized photoemission results

Spin-polarized photoemission results on the Ag/Fe(001) system described in detail elsewhere[5,9] are summarized in Figs. 2 and 3. Figure 2 shows the spin-integrated photoemission spectra and spin polarization for the clean Fe(001) surface and for the completion of integral numbers of Ag monolayers. The clean Fe(001) surface displays a feature at a binding energy 2.4 eV which has been identified as a minority-spin surface state residing in the Δ_1 *s-d* hybridization gap of the bulk band structure.[10] The evolution of this state into a magnetic quantum-well state is a main theme of this paper.

With each new monolayer, a new peak emerges at progressively higher energies. The binding energies of this feature relative to the Fermi energy are 2.4, 1.7, 1.0, and 0.3 eV for 0, 1, 2, and 3 monolayers of Ag, respectively. These various peaks are all of minority-spin character since, as is evident from Fig. 2, the position of each peak coincides with a minimum in the spin-polarization asymmetry. An actual decomposition into majority- and minority-spin spectra is shown in Fig. 3 for the one monolayer case. The prominent peak at 1.7 eV below E_F is clearly of minority spin. Note, however, in the majority-spin spectrum, there is a weak bump at 3.0 eV below E_F. Thus majority-spin features are not entirely absent.

B. Inverse photoemission

Ortega *et al.* have recently published[5] the results of extensive inverse photoemission studies on various overlayer systems including Ag/Fe(001). The results indicate a hierarchy of quantum-well states, one of which (the $\nu=1$ state defined below) matches very well with the state that has been observed using spin-polarized photoemission spectroscopy.[4] We make use of these results in Sec. III below.

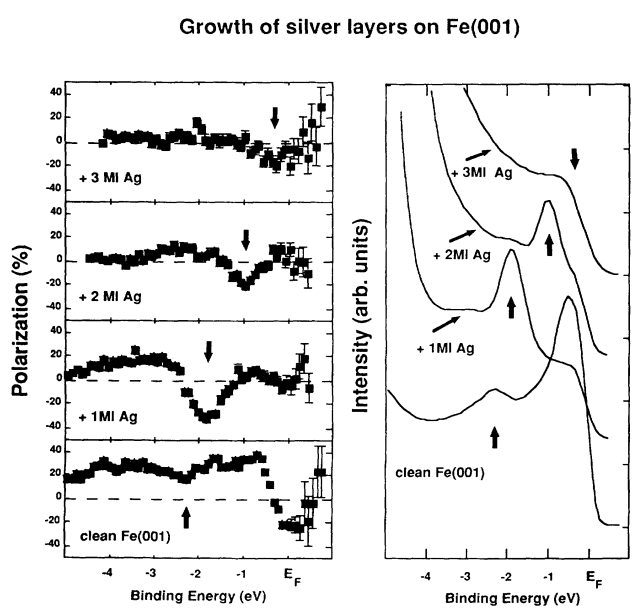

FIG. 2. Spin asymmetry and total spectra at integral monolayer coverages of Ag on Fe(001).

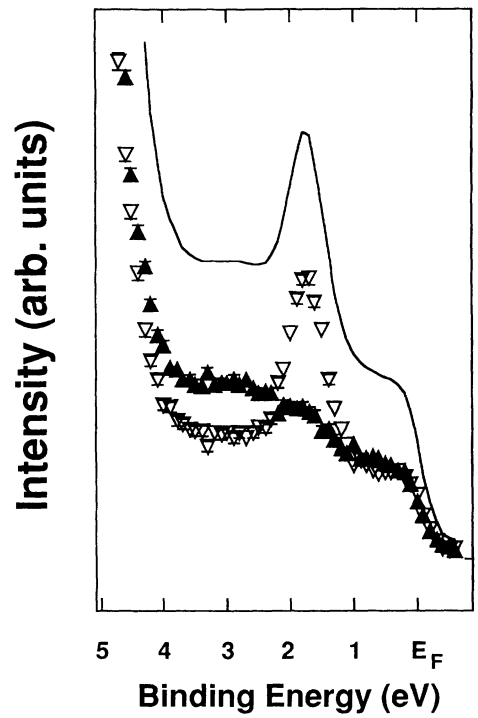

FIG. 3. Spin decomposition of the total photoemission spectrum for 1 monolayer Ag (full curve) into majority (▲) and minority (▽) components.

III. QUANTUM-WELL ANALYSIS

We invoke the phase-accumulation model[11,12] which has worked so successfully in the interpretation of image states and surface states on clean metals and of quantum-well-type states in layered noble-metal systems.[13] The quantization condition for the existence of such states is

$$\phi_C + 2kd + \phi_B = 2\pi n \ , \tag{1}$$

where ϕ_C and ϕ_B are the phase changes on reflection at the crystal and at the surface barrier; and where k is the wave vector of a free electron propagating in a layer of thickness d. The total phase accumulation must be an integral multiple of 2π. This is nothing more than the problem of a particle in a box of width d, with ϕ_C and ϕ_B embodying the wave-function matching condition at the boundaries of the box. The quantum number n is the number of nodes or half-wavelengths that the wave function has inside the box.

In growing successive overlayers we are increasing d in units of the layer spacing a; thus $d=ma$, where m is an integer. In the case of Ag discussed here, the wave vector k is close to the Fermi wave vector k_F which in turn is close to the Brillouin zone wave vector $k_{BZ}=\pi/a$. An

increment of a in the thickness of the overlayer will fall slightly short of half an electron wavelength. Equation (1) can therefore be satisfied by a small increment $k \rightarrow k + \Delta k$, and by adding a half-wavelength.

$$\phi_C + \phi_B + m2ka = 2\pi n \ , \tag{2}$$

$$\phi_C + \phi_B + (m+1)2(k+\Delta k)a = 2\pi(n+1) \ , \tag{3}$$

whence (ignoring for the moment the variations of ϕ_C, ϕ_B with energy),

$$\Delta k = (k_{\mathrm{BZ}} - k)/(m+1) \ . \tag{4}$$

Thus k and the energy of the state will increase with increasing layer thickness, as observed. The wave vector k approaches k_{BZ} in decreasing fractions, $(m+1)^{-1}$, of the remaining distance, $(k_{\mathrm{BZ}} - k)$, to be covered. At large values of m, the energy of a quantum-well state is expected to level off at the energy $E(k_{\mathrm{BZ}})$ characteristic of the zone boundary which, in the particular case of Ag(001), corresponds to the p-like state of $X_{4'}$ symmetry. These results are elaborated in Fig. 4, which shows a graphical solution of Eq. (2). Curves representing $2\pi n - \phi_C - \phi_B$ advance arithmetically with increasing n. Curves for $2kma$ advance multiplicatively with m.

To generate ϕ_B we have used the WKB approximation[14]

$$\phi_B/\pi = \left[\frac{3.4\ (\mathrm{eV})}{E_V - E} \right]^{1/2} - 1 \ , \tag{5}$$

where E_V is the vacuum level. This approximation is known to work rather well at $\bar{\Gamma}$ for d-band metals with inverted s-p gaps.[12] To generate ϕ_C, we have used the purely empirical formula:[15]

$$\phi_C = 2 \arcsin[(E - E_L)/(E_U - E_L)]^{1/2} - \pi \ , \tag{6}$$

where E_U and E_L are, respectively, the energies of the upper and lower edges of the hybrization gap in Fe. It is known on very general grounds[16] that ϕ_C must increase by π on traversing a gap. The empirical approximation of Eq. (6) has the desired sigmoid form, varying rapidly with E at the band edges. To generate the $2kma$ curves we have calculated k from the standard two-band nearly-free electron expression:

$$k(E) = G^{1/2} - [(G+E) - (4GE + v_g^2)^{1/2}]^{1/2} \tag{7}$$

whose parameters G and v_g are chosen ($G \equiv \hbar^2 k_{\mathrm{BZ}}^2/2m = 9.08$ eV, $v_g = 1.67$ eV) to reproduce the known band energies ($\Gamma_1 = E_F - 5.5$ eV), $X_{4'} = E_F + 1.9$ eV, and $X_1 = E_F + 5.24$ eV) for Ag.

The graphical solutions for the electron energies are indicated by the filled circles in Fig. 4. It is seen that the appropriate quantum number in the classification of these states is not n or m, but rather $\nu \equiv m - n$. In this classification scheme, the thickness versus energy relation may be written

$$\frac{D_\nu(E)}{a} = \frac{[\phi_C(E) + \phi_B(E)]/2\pi + \nu}{(1 - k(E)/k_{\mathrm{BZ}})} \ , \tag{8}$$

which is similar to Eq. (4) of Ref. 5. Note that this follows immediately from Eqs. (2) and (3) of this paper without need of the envelope function and carrier wave introduced in Ref. 5. The envelope function is a secondary consideration which arises when one examines the QW wave functions in the two-band NFE model. An Appendix is offered below which puts the envelope function in its proper perspective.

Comparison with the experimental photoemission and inverse photoemission results is shown in Fig. 5. The points of agreement and disagreement are now discussed. Points of agreement are as follows.

(1) Multiplicity of states. The model predicts the hierarchy of QW states advancing upwards in energy with increasing overlayer thickness. The values of the energies are reproduced very well.

(2) Saturation at $X_{4'}$. The energies of the states level off at sufficiently large thickness. The maximum energy of the $\nu = 0$ state observed in the inverse photoemission experiments is 1.5 eV considerably lower than the 1.9 eV of the $X_{4'}$ level. Band calculations are not all in agreement on this level, however. An alternative calculation[17] places $X_{4'}$ at 1.6 eV in much closer agreement with experiment. The $\nu = 1$ level at higher thicknesses also falls below our quantum-well prediction. Ortega *et al.* offer a quantum-well model which is in better agreement for the $\nu = 1$ level. In that model, however, the energy dependence of the combination $\phi_C + \phi_B$ is treated as linear with an adjustable slope. We have confined ourselves here to functions for $\phi_C + \phi_B$ which are physically motivated and which have corroboration from other work.[12,15]

(3) Periodicity of Fermi level crossovers. The $\nu = 1$ state is observed to cross E_F between 3 and 4 Ag monolayers. This is in good agreement with the $m = 3.8$ predicted by the model. Subsequent crossovers are predicted to occur with a period given by

$$\Delta m = (1 - k_F/k_{\mathrm{BZ}})^{-1} \tag{9}$$

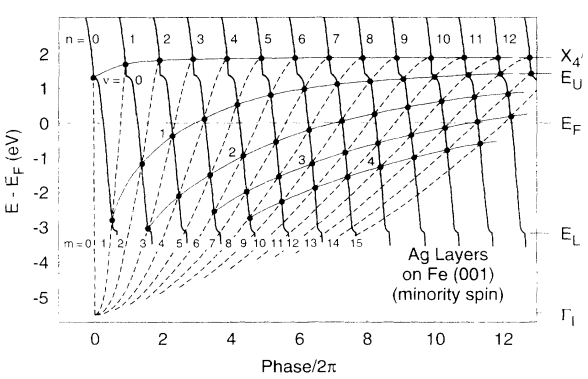

FIG. 4. Graphical solutions (filled circles) for the energies of quantum-well states of Ag overlayers on Fe(001) using the phase-accumulation model. Full bold curves represent the phase $2\pi n - \phi_C - \phi_B$, and advance arithmetically with increasing node number n. Dashed curves represent the quantum-well phase accumulation $m2ka$, and advance multiplicatively with layer number m. States characterized by the quantum number $\nu (\equiv m - n)$ are connected by the full thin curves. The $\nu = 1$ state crosses E_F just below 4 monolayers.

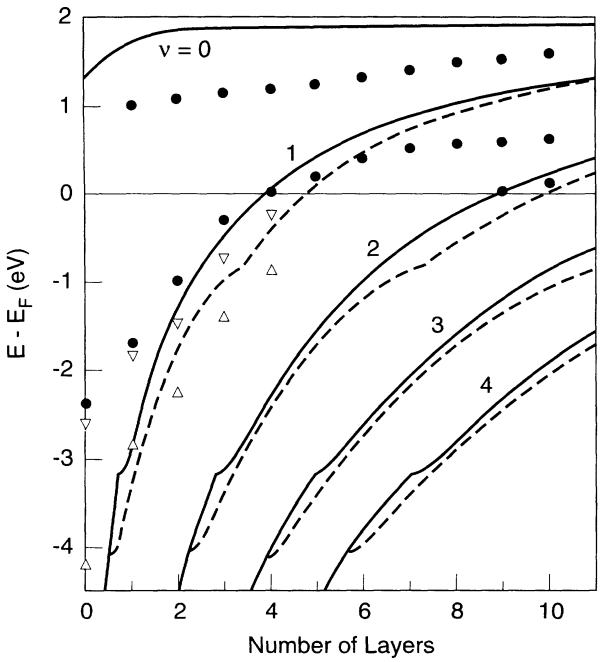

FIG. 5. Comparison between theory and experiments for the energies of surface states and quantum-well states for Ag overlayers on Fe(001) as a function of overlayer thickness. Filled circles represent the photoemission data of this paper ($E < E_F$) and the inverse photoemission data of Ref. 5 ($E \geq E_F$). Open triangles are the energies of majority (△) and minority (▽) spin states generated by tight-binding calculations.

which, for our particular parameters, comes to $\Delta m = 5.2$ layers. Thus the observed crossover of the $\nu = 2$ state at 9 layers is in good agreement. As noted previously,[5] this period also agrees well with the period for the alternation between ferromagnetic and antiferromagnetic coupling in Ag/Fe multilayer systems. The periodicity of Eq. (9) is identical with that given by "aliasing" and Fermi-surface spanning-vector models[18] such as that of Bruno and Chappert.[19] It is not necessary to impose a long period "envelope function" as in Ref. 5. The long period is an aliasing or "node-dropping" phenomenon whereby new QW solutions at E_F are generated by adding Δm new layers but only $\Delta m - 1$ new half-wavelengths to the wave function. (We are dealing here with the simplest case of a nearly spherical Fermi surface. With more complicated Fermi surfaces the possibility of multiple periodicities arises.[20])

Points of disagreement are as follows.

(1) Bare substrate. The quantum-well model fails to predict the existence of a surface state within the hybridization gap on the bare Fe(001) substrate. This is a serious failing since this surface state is conspicuous in the spin-polarized photoemission data.[10] It appears to be closely connected with the $\nu = 1$ quantum-well state and confers its spin character to it.

(2) $\nu = 0$ surface resonance. The predicted $\nu = 0$ state is *not* observed on the bare substrate. This state is the Shockley surface resonance associated with the inverted *s-p* band gap.[12] It is merely an incipient resonance on the Fe(001) surface since its energy lies far below the lower edge of the gap. On the Ag(001) surface, on the other hand, the state lies quite close to the lower edge ($X_{4'}$) of the gap (see Fig. 1). This incipient Shockley surface resonance evolves into an observable resonance with increasing Ag layer thickness.

(3) Spin polarization. The model predicts QW states of *both* spins, but only minority spins are observed strongly. For the minority-spin system, the observed states near E_F lie within the *s-d* hybridization gap of the Fe substrate. For the majority-spin system, E_F lies above the band gap. Thus QW confinement applies strictly only to the minority-spin system and this has been offered as the reason for the absence of a majority-spin feature in the photoemission spectra.[5]

IV. TIGHT-BINDING SIMULATION

To gain insight into the wave function and spin character of the interface states, we have performed empirical tight-binding model calculations. Described in greater detail elsewhere,[7,8] these calculations take parameters associated with a tight-binding fit to the appropriate paramagnetic band structure, split the on-site spin-dependent energies for the *d* blocks of the Hamiltonian by an amount Δ, calculate the spin-dependent densities of states, and integrate up to the Fermi level to obtain the resulting layer-dependent moments. A self-consistent solution is sought such that the Stoner criterion is satisfied for each layer. Two-center nonorthogonal parameters are taken from the compilation of Papaconstantopoulos[9] with the on-site diagonal energies adjusted to bring the Fermi levels into alignment. For the clean surface, the tight-binding calculations yield a surface state whose binding energy is in good agreement with first-principles full-potential linearized augmented plane wave calculations[21] and with experiment. With successive additions of Ag overlayers, this state advances to higher energies again in agreement with experiment. The actual energies are indicated by the open triangles in Fig. 5.

Results for the layer-by-layer charge densities are shown in Fig. 6 for the minority-spin surface state and its evolution with increasing Ag thickness. These results were obtained for a 13-layer Fe slab with symmetric accretions of Ag layers on both sides. The calculations indicate that the charge density of this state extends throughout the Ag layer. It is appropriate, therefore, to regard this state as a QW state confined within the Ag overlayer. We now explore this proposition by examining the eigenvectors (i.e., orbital decomposition) of the TB model.

In agreement with a related study of the related Cu/Co(001) system, we find that the quantum-well states have significant *d* character.[22] Orbital amplitudes of *s* and d_{z^2} basis states are shown in Fig. 7 for the eigenstates identified with the experimentally observed peaks. These calculations used a 7-layer Fe slab with symmetric accretions of Ag layers on both sides. In this symmetric geometry, the surface–interface–quantum-well states are generated in almost degenerate symmetric and antisymmetric pairs. We plot in Fig. 7 amplitudes of the *symmetric* partner, the intent being to show the degree of

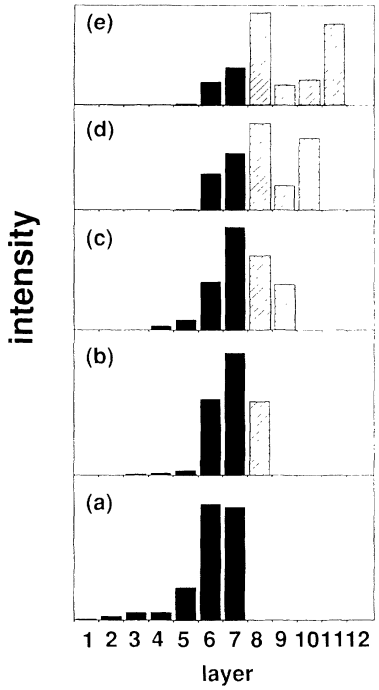

FIG. 6. Charge densities per layer generated by tight-binding slab calculations for Ag overlayers on Fe(001). The calculations treat a 13-layer Fe slab (a) with symmetric additions of Ag monolayers (b)–(e). The layers are numbered outward from the center of the slab.

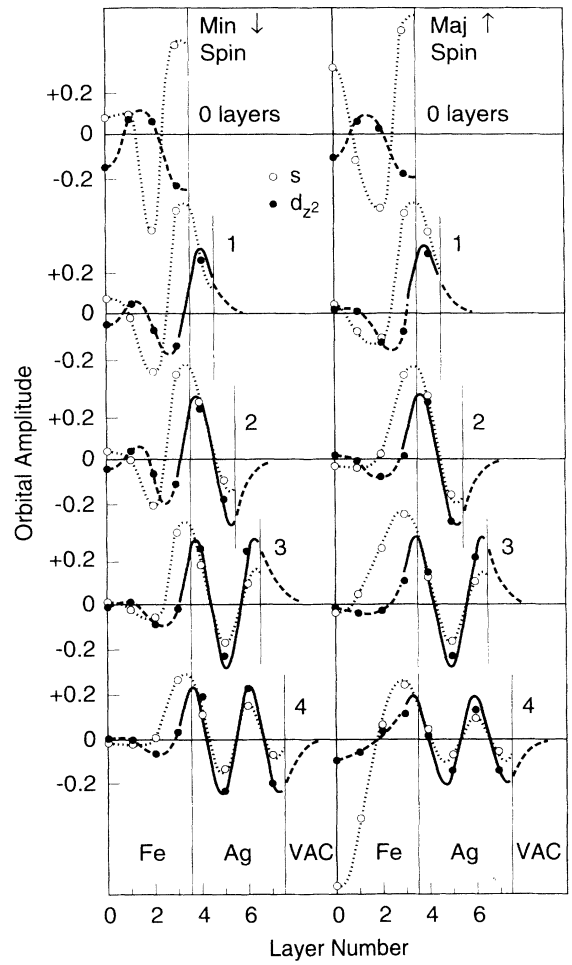

FIG. 7. Eigenvector amplitudes generated by tight-binding simulations of the surface states and quantum-well states for Ag overlayers on Fe(001). Filled and open circles represent, respectively, "s" and "d_{z^2}" orbital amplitude. The full curves are sinusoids with periodicity given by Eq. (7). The dashed and dotted curves have no theoretical significance, and are intended merely to guide the eye.

wave-function penetration into the Fe slab. (The antisymmetric partner necessarily vanishes on the central layer of the Fe slab.)

At the larger Ag coverages, the TB model delivers the essential features of the QW model. The full curves in Fig. 7 are sinusoids whose period is given by Eq. (7). The match with the "s" orbital amplitudes (full circles in Fig. 7) is very good. Thus, the TB model contains within it the QW model. Specifically, the wave function acquires an extra node with the addition of each new Ag monolayer.

At the lower Ag coverages, we can track the way in which the quantum-well states merge with the intrinsic surface states of the substrate. For the 2-, 3-, and 4-layer Ag coverages, it is apparent from Fig. 7 that the s and d_{z^2} orbital amplitudes oscillate more or less in phase and with the same sign; that is to say, we have a *bonding* s-d_{z^2} configuration in the Ag overlayer. The orbital configuration in the outermost layer of the bare Fe substrate is s-d_{z^2} antibonding with a preponderance of d over s amplitude. (The eigenvectors contain a substantial p_z component which has been omitted from Fig. 7 for reasons of clarity.) With increasing Ag coverage, the s-d_{z^2} configuration in the outermost Fe layer changes eventually from antibonding to bonding. This progression is presumably the physical ingredient that is lacking in the QW model.

At 4 monolayers of Ag the majority-spin QW state occurs at a energy above the top of the Fe s-d hybridization gap. The wave function then penetrates into the substrate and can be seen in Fig. 7 as the very large amplitude on the central Fe layer of the slab. This result lends credence to the suggestion[5] that this is the physical explanation for the absence or weakness of majority-spin states in the measured spectra.

We may conclude that the TB model accounts satisfactorily for the energies of surface states on clean Fe(001), for the energies of interface states at low Ag coverage, and for the eventual evolution into QW states at high coverage. Both the TB and QW models predict states of both minority and majority spin. The large disparity in intensity of minority- and majority-spin features in the measured spectra is only tentatively understood and would be worthy of further experimental and theoretical study. It would also be desirable to perform off-normal measurements so as to probe regions of $k_{\parallel}$-space where the Fermi surface departs from sphericity.

ACKNOWLEDGMENTS

It is a pleasure to acknowledge discussions with A. Clarke and M. Weinert. This work was supported in part by the U.S. Department of Energy under Contract No. DE-AC02-76CH00016 and the National Science Foundation under Materials Research Group Contract No. DMR-86-03304.

APPENDIX

We address here the inclusion of band structure *within* the QW using the two-band NFE model. It has already proved advantageous in the elaboration of the phase-accumulation model to use the $k(E)$ generated by the two-band NFE model rather than the free electron k. We now examine the QW wave functions, discuss the envelope function, and rederive the phase model.

In the two-band NFE model, the electron wave function is written

$$\psi=\alpha_0 e^{ikz}-\alpha_g e^{i(k-g)z} , \tag{A1}$$

where g is a reciprocal lattice vector. This is simply a forward traveling plane wave of amplitude α_0 interfering with a back-diffracted wave of amplitude α_g. The amplitudes are given by

$$\alpha_0=c_g/(c_g^2+v_g^2)^{1/2} , \tag{A2}$$

$$\alpha_g=v_g/(c_g^2+v_g^2)^{1/2} , \tag{A3}$$

with

$$c_g=[(E_0-E_g)^2/4+v_g^2]^{1/2}-(E_0-E_g)/2 , \tag{A4}$$

where $E_0=\hbar^2k^2/2m$ and $E_g=\hbar^2(k-g)^2/2m$. We are restricting our attention here to the lower energy band for the case of a repulsive pseudopotential ($v_g>0$), and we take the $z=0$ origin on an atom center.

The complex conjugate ψ^* would be an equally acceptable wave function, but having the propagation directions reversed. For the purpose of fitting wave functions in quantum wells, it is convenient to work with a real cosinelike function $\psi_c\equiv(\psi+\psi^*)/2$ and a real sinelike function $\psi_s\equiv -i(\psi-\psi^*)/2$. Writing $k\equiv g/2-\kappa$, we have

$$\psi_c=(\alpha_0+\alpha_g)\sin(gz/2)\sin(\kappa z) +(\alpha_0-\alpha_g)\cos(gz/2)\cos(\kappa z) , \tag{A5}$$

$$\psi_s=(\alpha_0+\alpha_g)\sin(gz/2)\cos(\kappa z) -(\alpha_0-\alpha_g)\cos(gz/2)\sin(\kappa z) , \tag{A6}$$

These functions are illustrated in Fig. 8 for representative values of k using parameters appropriate to Ag(001). Also shown are the charge densities $\rho\equiv|\psi_c\pm i\psi_s|^2$ of the associated Bloch functions.

Near the zone boundary [see Fig. 8(a)] the wave function displays an amplitude modulation having a long period envelope with wave vector κ. Near the zone center, on the other hand [see Fig. 8(c)], we have $\psi_c\sim\cos(kz)$ and $\psi_s\sim\sin(kz)$, but with a small short-wavelength ripple. Figure 8(b) corresponds roughly to the situation at the Fermi level where we are trying to fit 4 half-wavelengths into 5 layers ($\nu=1$ state), 8 half-wavelengths into 10 layers ($\nu=2$ state), and so on.

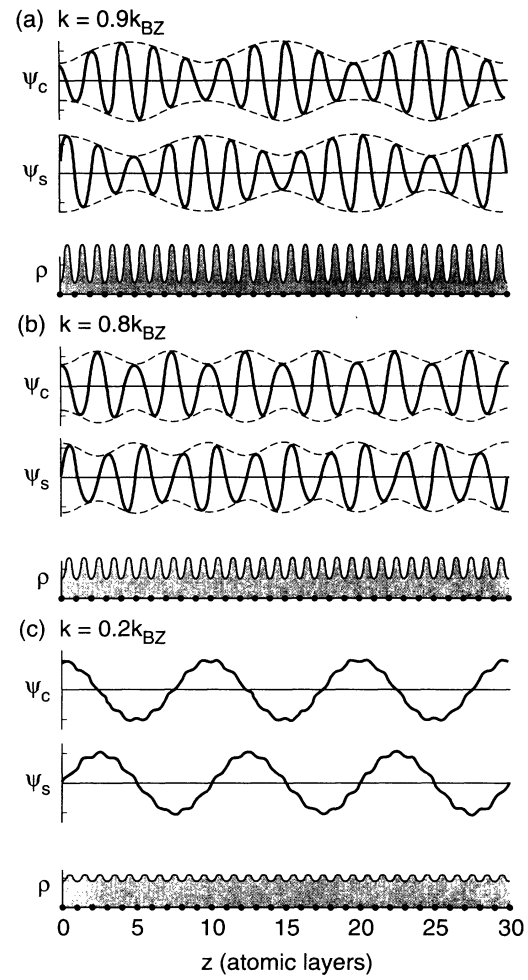

FIG. 8. Wave functions generated by the two-band NFE model for Ag(001) for various values of wave vector k: (a) $k=0.9k_{BZ}$; (b) $k=0.8k_{BZ}$; and (c) $k=0.2k_{BZ}$. ψ_c and ψ_s are the cosinelike and sinelike QW functions, respectively, and ρ is the charge density $|\psi_c\pm i\psi_s|^2$ of the associated Bloch functions. The dashed curves in (a) and (b) indicate the envelope function.

Let us now consider a QW in which the matching planes, $z=z_C$ and $z=z_B$, are set at half a layer-spacing beyond the outermost atomic layers. Let l_C and l_B be the respective logarithmic derivatives of the wave functions outside the QW evaluated at z_C and z_B. It is then easy, using a linear combination of ψ_c and ψ_s within the QW, to derive the following quantization condition on the envelope wave vector κ:

$$\tan\kappa(z_B-z_C)=\frac{-l_C/\xi+l_B/\xi}{1+(l_C/\xi)(l_B/\xi)} , \tag{A7}$$

where

$$\xi=(\alpha_0+\alpha_g)[\alpha_0(g/2-\kappa)-\alpha_g(g/2+\kappa)] . \tag{A8}$$

Defining phases: $\tan(\phi_C^*/2)\equiv -l_C/\xi$ and $\tan(\phi_B^*/2)$

$\equiv +l_B/\xi$, we have

$$\tan \kappa d = \tan(\phi_C^*/2 + \phi_B^*/2) \tag{A9}$$

or

$$\phi_C^* + \phi_B^* - 2\kappa d = -2\pi\nu \ , \tag{A10}$$

where ν is an integer. This, expressed here in more rudimentary mathematics, is the result published by Beckman, Klaua, and Meinel.[23] Remembering that $\kappa = g/2 - k$ and that $gd = 2\pi m$, we have

$$\phi_C^* + \phi_B^* + 2kd = 2\pi(m - \nu) = 2\pi n \ , \tag{A11}$$

and so we retrieve the phase accumulation model with quantum numbers n, m, and ν having the same meanings as above, but with modified phase parameters ϕ_C^* and ϕ_B^*. For a QW with a flat potential ($v_g = 0$), the phases would be given by $\tan(\phi_C/2) = -l_C/k$ and $\tan(\phi_B/2) = +l_B/k$. Replacing k by ξ is easily done but is a correction which, given the crudity of our approximations for ϕ_C and ϕ_B, can be safely ignored for the purposes of this paper. The modifications become important only on approaching very close to the zone boundary since $\xi \to 0$ as $k \to k_{BZ}$.

[1]See, for example, L. M. Falicov, Phys. Today, **45** (10), 46 (1992).

[2]M. N. Baibich, J. M. Broto, A. Fert, F. Nguyen Van Dau, F. Petroff, P. Etienne, C. Creuzet, A. Friederich, and J. Chazelas, Phys. Rev. Lett. **61**, 2472 (1988).

[3]S. S. Parkin, N. More, and K. P. Roche, Phys. Rev. Lett. **64**, 2304 (1990).

[4]N. B. Brookes, Y. Chang, and P. D. Johnson, Phys. Rev. Lett. **67**, 354 (1991).

[5]J. E. Ortega, F. J. Himpsel, C. J. Mankey, and R. F. Willis, Phys. Rev. B **47**, 1540 (1993).

[6]P. D. Johnson, Y. Chang, and N. B. Brookes (unpublished).

[7]P. D. Johnson, N. B. Brooks, Y. Chang, and K. Garrison (unpublished).

[8]N. B. Brooks, Y. Chang, and P. D. Johnson (unpublished).

[9]D. A. Papaconstantopoulos, *Handbook of the Band Structure of Elemental Solids* (Plenum, New York, 1986).

[10]N. B. Brooks, A. Clarke, P. D. Johnson, and M. Weinert, Phys. Rev. B **41**, 2643 (1990).

[11]P. M. Echenique and J. B. Pendry, J. Phys. C **11**, 2065 (1978).

[12]N. V. Smith, Phys. Rev. B **32**, 3549 (1985).

[13]M. A. Muellar, T. Miller, and T. C. Chiang, Phys. Rev. B **41**, 5214 (1990), and references therein.

[14]E. G. McRae and M. L. Kane, Surf. Sci. **108**, 435 (1981).

[15]P. M. Echenique and J. B. Pendry, Prog. Surf. Sci. **32**, 111 (1989).

[16]J. B. Pendry and S. B. Gurman, Surf. Sci. **49**, 87 (1975).

[17]H. Eckardt, L. Fritsche, and J. Noffke, J. Phys. F **14**, 97 (1984).

[18]D. M. Edwards, J. Mathon, R. B. Muniz, and M. S. Phan, Phys. Rev. Lett. **67**, 493 (1991); D. M. Deaven, D. S. Rokhsar, and M. Johnson, Phys. Rev. B **44**, 5977 (1991); F. Herman, J. Sticht, and M. Van Schilfgaarde, J. Appl. Phys. **69**, 4783 (1991).

[19]P. Bruno and C. Chappert, Phys. Rev. Lett. **67**, 1602 (1991); Phys. Rev. B **46**, 261 (1992).

[20]S. N. Okuno and K. Inomata, Phys. Rev. Lett. **70**, 1711 (1993), and references therein.

[21]S. Ohniski, M. Weinert, and A. J. Freeman, Phys. Rev. B **30**, 36 (1984); M. Weinert (private communication).

[22]K. Garrison, Y. Chang, and P. D. Johnson, Phys. Rev. Lett. **71**, 2801 (1993).

[23]A. Beckman, M. Klaua, and K. Meinel, Phys. Rev. B **48**, 1844 (1993).

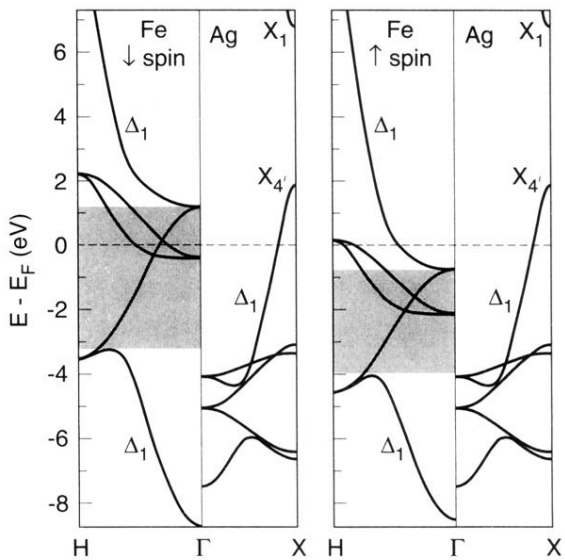

FIG. 1. Energy bands of Fe and Ag along the Δ direction for both minority (↓) and majority (↑) spins. The toned areas indicate the range of the *s-d* hybridization gap in Fe for states of Δ_1 symmetry.

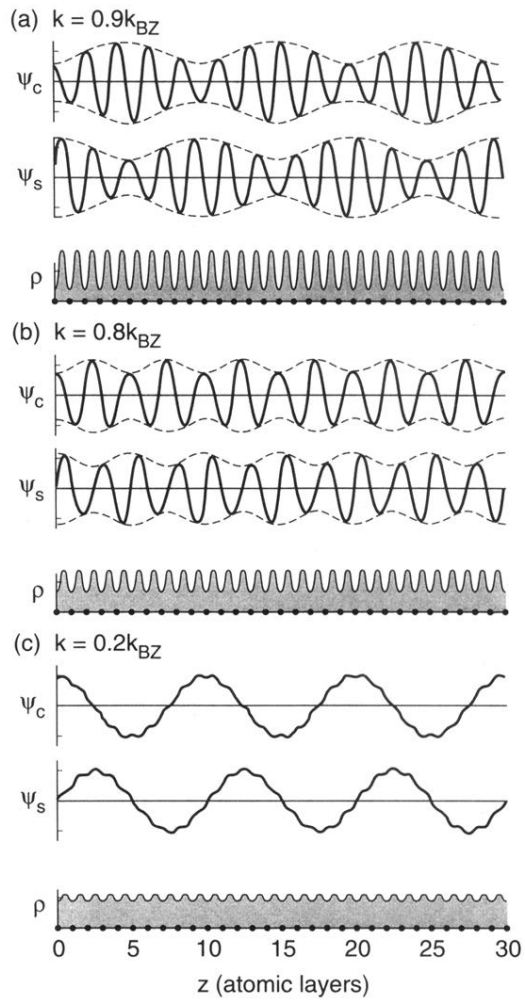

FIG. 8. Wave functions generated by the two-band NFE model for Ag(001) for various values of wave vector k: (a) $k=0.9k_{\mathrm{BZ}}$; (b) $k=0.8k_{\mathrm{BZ}}$; and (c) $k=0.2k_{\mathrm{BZ}}$. ψ_c and ψ_s are the cosinelike and sinelike QW functions, respectively, and ρ is the charge density $|\psi_c \pm i\psi_s|^2$ of the associated Bloch functions. The dashed curves in (a) and (b) indicate the envelope function.